

<https://helda.helsinki.fi>

Equilibrium simulation and driving factors of dissolved oxygen in a shallow eutrophic Inner Mongolian lake (UL) during open-water period

Zhang, Fan

2022-06-01

Zhang , F , Shi , X , Zhao , S , Arvola , L , Huotari , J & Hao , R 2022 , ' Equilibrium simulation and driving factors of dissolved oxygen in a shallow eutrophic Inner Mongolian lake (UL) during open-water period ' , Water Science and Technology: Water Supply , vol. 22 , no. 6 , pp. 6013-6031 . <https://doi.org/10.2166/ws.2022.217>

<http://hdl.handle.net/10138/345977>
<https://doi.org/10.2166/ws.2022.217>

cc_by
publishedVersion


Downloaded from Helda, University of Helsinki institutional repository.

This is an electronic reprint of the original article.

This reprint may differ from the original in pagination and typographic detail.

Please cite the original version.

Equilibrium simulation and driving factors of dissolved oxygen in a shallow eutrophic Inner Mongolian lake (UL) during open-water period

Fan Zhang ^a, Xiaohong Shi^{a,*}, Shengnan Zhao^a, Lauri Arvola^b, Jussi Huotari^b and Ruonan Hao^a

^a College of Water Conservancy and Civil Engineering, Inner Mongolia Agricultural University, Hohhot 010018, China

^b Lammi Biological Station, Ecosystems and Environment Research Programme, Faculty of Biological and Environmental Sciences, Helsinki University, Lammi FI-16900, Finland

*Corresponding author E-mail: imaushixiaohong@163.com

 FZ, 0000-0002-8746-3715

ABSTRACT

A water quality monitoring buoy installed in the center of the eutrophic shallow lake Ulansuhai was used to explore the dissolved oxygen (DO) balance. A revised DO model for shallow eutrophic lakes was applied to identify trends in the lake's DO content during the non-frozen period and determine the equilibrium relationship of DO in the water body. The coefficient of determination and the Nash efficiency of the model proved the feasibility of the model. The main drivers affecting the DO balance of the lake were photosynthesis, aeration and the lateral movements of oxygen-rich water, which accounted for 49.28, 14.72 and 36%, respectively, whereas respiration and sediment oxygen consumption, on the other hand, accounted for 1.56 and 98.44%, respectively. These findings suggest that photosynthesis and sediment oxygen consumption dominate the DO balance in eutrophic shallow lakes. A trend analysis of the average oxygen production and consumption rates indicated a maximum of 0.22 mg/L-h for photosynthesis and 0.20 mg/L-h for sediment oxygen consumption. A correlation analysis showed that water temperature was involved in changing the DO level of the lake mainly by affecting the oxygen consumption process.

Key words: dissolved oxygen equilibrium, model simulation, online monitoring, open-water period, shallow eutrophic lakes

HIGHLIGHTS

- Continuous DO data were obtained by an on-line monitoring instrument with high frequency, and the data were simulated.
- A model of DO in a shallow water eutrophication lake is improved and successfully applied to typical lakes in the study area.
- The main driving factors of DO were found out and their variation range was determined.

1. INTRODUCTION

The dissolved oxygen (DO) content of water bodies is an important indicator of water quality (Sánchez *et al.* 2007). The activity of many aquatic organisms such as several fish species are inhibited when the concentration of DO in a water body drops below 5 mg/L (Huang *et al.* 2019), and concentrations below 2 mg/L have been shown to accelerate the anaerobic decomposition of organic material in water bodies and sediments releasing excessive levels of nitrogen and phosphorus, implying a status of eutrophication (Xu & Xu 2015). The rate of recovery of DO in natural water bodies determines their self-purification ability. If the recovery rate is fast, this indicates a strong self-purification ability, and if not, this indicates a weak self-purification ability; if a water body becomes severely polluted, it may even lose its self-purification ability entirely (Chinyama *et al.* 2016). The DO levels and understanding the mechanisms driving DO are essential if we are to manage our lake water environments effectively and maintain a healthy water ecological balance.

The changing levels of DO in water bodies are driven by several dynamic processes of continuous depletion and replenishment, and therefore DO concentration is a result of interactions of multiple factors (Houser *et al.* 2015), and there are many environmental factors such as the water temperature, radiation, wind speed, and nutrient level of the water body (Song *et al.* 2019). Trends in the level of DO are difficult to predict given these complex and variable environmental and meteorol. In recent years there has been a great deal of research on the topic and a number of numerical models have now been proposed to predict levels of DO in rivers, lakes and ponds under different meteorological and hydrological conditions. Chapra & Di

This is an Open Access article distributed under the terms of the Creative Commons Attribution Licence (CC BY 4.0), which permits copying, adaptation and redistribution, provided the original work is properly cited (<http://creativecommons.org/licenses/by/4.0/>).

Toro (1991) estimated riverine reoxygenation, primary productivity, and respiration rates for Michigan's Grand River in the USA using the Delta method, presenting their numerical solution in graphical form. In rivers, the factors regulating DO balance consist of three main dynamic processes, namely exchange at the atmosphere-water interface, photosynthesis, and respiration (Odum 1956; Schurr & Ruchti 1977; Parkhill & Gulliver 1999); but the faster flow rates of rivers mean better water mixing and DO transfer between water and atmosphere, which in turn means that their DO is less influenced by sediment and substrate, which are important in the oxygen balance of lakes (Murniati *et al.* 2015). Malve *et al.* (2005) modeled winter respiration in Tuusulanjärvi Lake, Finland, as total DO consumption in the lake water, using a Bayesian model to estimate and predict its oxygen status. Terry *et al.* (2017) used the CE-QUAL-W2 model to target simulations of sediment oxygen consumption changes at the sediment-water interface in a prairie lake in Saskatchewan, Canada, obtaining more accurate DO simulations in winter relative to summer. Unfortunately, those studies focused primarily on oxygen consumption factors in the water column, and did not consider the other factors driving DO changes. Hull *et al.* (2008) developed a continuous dissolved oxygen kinetic model to predict DO in a coastal lagoon in Italy and tested it in the laboratory to confirm the environmental elements driving DO changes. However, due to the lack of high frequency data collection or sufficient experimental data, they were not able to conduct an in-depth study of the DO kinetics. Most of the water column DO simulations reported to date have focused on rivers, deep lakes and reservoirs, with only few examining shallow and eutrophic lakes. Yet only a very few studies have sought to quantify the factors driving DO variability in lakes due to the large variability between different lakes and the key drivers. The high variability complicates the development of DO models considerably (Stefan & Fang 1994).

After careful evaluation, a high-frequency DO model applicable to shallow eutrophic lakes was chosen for this study (Xu & Xu 2016). This deterministic model considers dynamic changes in both the oxygen source and the oxygen consumption, and can be applied to simulations and predictions of DO levels in lakes. The improved model taking into account the specific human, climatic, geographical, and land-use characteristics of the study area, it serves as a useful tool for studying the DO dynamics of the lake and then to be able to analyze the DO balance in large bodies of lake water. The main objective of this study was to explore the high-frequency model of DO dynamics in Ulansuhai Lake, identifying the driving forces governing the level of DO in the lake and ultimately, providing an effective basis for future decisions regarding the scientific management and health assessment of the lake.

2. MATERIALS AND METHODS

2.1. Study area description

The study area, Ulansuhai Lake (40°36'–41°03'N, 108°43'–108°57'E) is located close to Bayannur City, Inner Mongolia, at the end of the Hetao Plain in northwestern China. Lying between the Yellow River to the south and Wolf Mountain to the north (Figure 1), it is a rare shallow lake with an annual average water depth of 1.8 m and a overall area of 293 km², but the open water accounts for only about a third of the area, and the overall length of the lake's shoreline is about 130 km. As a rare large-scale multi-functional grassland lake in this desert and semi-desert region, Ulansuhai Lake is not only responsible for much of the regional water regulation and storage, but is also the only water body and drainage channel for the return of farmland runoff in the Hetao Irrigation District of Inner Mongolia (Yu *et al.* 2007). In addition, studies have shown that due to the high frequency of human activity in the area in recent years (Quan *et al.* 2020), most of the water bodies within Ulansuhai Lake are suffering from a mild to moderate degree of eutrophication.

Ulansuhai Lake has a typical mid-temperate continental arid and semi-arid monsoon climate, with hot summers and little rain, and cold, dry winters. The long-term annual average temperature around Ulansuhai Lake is 7.3 °C. The monthly average air temperature ranges from 24.1 °C in the hottest month (July) to the coldest month (November) at 4.4 °C. During the study period (July-early November), the average temperature was 14.9 °C. The lake enters a five-month ice-cover period at the beginning of November each year, only melting completely in April of the following year. The local multi-year average precipitation is 224 mm, and the total precipitation during the study period is 321 mm, ranging from 144 mm in August to 0.26 mm in October. The annual average wind speed is 0.44 m/s, so the lake is subjected to almost constant low wind speeds.

2.2. Wind speed and radiation data collection

The meteorological data was collected with the HOBO automatic weather station at Honggebu (at point WS1) and the Campbell automatic weather station located at the Ulansuhai Lake National Ecological Station (at point WS2), which are about

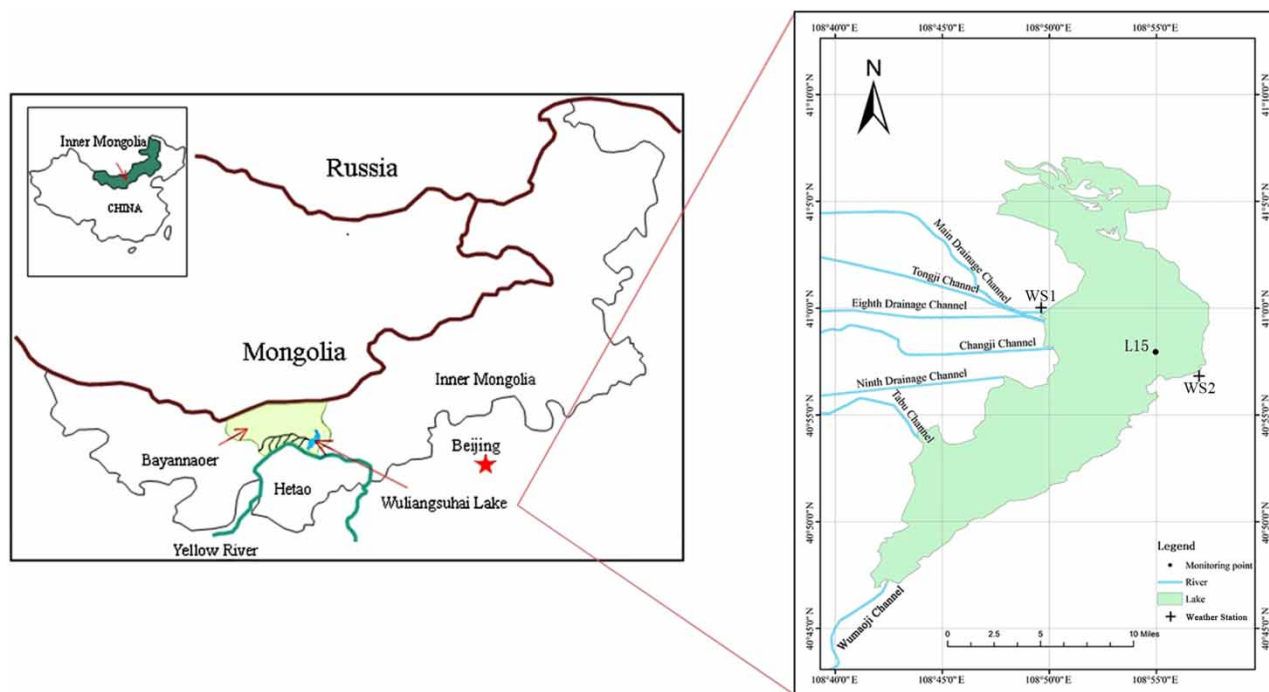


Figure 1 | The geographical location and monitoring point on Ulansuhai Lake.

8 km and 4 km away from the measurement point at *L15*, respectively (Figure 1). The hourly measurements were collected by two meteorological collectors and collected 5 months of continuous meteorological data, including wind speed, solar radiation, and photosynthetically active radiation. After feasibility analysis of these meteorological data, which were utilized for the oxygen production modeling calculation of photosynthesis and aeration.

2.3. DO, chlorophyll-a, and water temperature data

In July 2020, the water quality online monitoring buoy was placed at the *L15* point (40°58'N, 108°55'E) in the center of Ulansuhai and the buoy was equipped with a Yosemite water quality multi-parameter sensor (as shown in Figure 2). The data was collected by the YDOC GSM collector and uploaded to the Masinotek EMMI environmental monitoring system. The sensor was located 95 cm below the water surface, collecting and recording water quality data every hour, including DO concentration, chlorophyll-a concentration, and water temperature as well as other water quality indicators. A total of 2,921 hours of water quality data were collected during the study period from July to November. The sensor was calibrated in the laboratory before being deployed in the lake, and the equipment was cleaned and maintained at the end of each month during the monitoring period to ensure the stability and reliability of the data collected.

3. DO EQUILIBRIUM MODEL BASED ON THE CONDITIONS IN ULANSUHAI LAKE

3.1. DO model construction

The changing levels of DO in a body of water are governed by a dynamic equilibrium process of continuous consumption and replenishment. The hourly change in the DO concentration (Xu & Xu 2016) is expressed as:

$$DO_t = DO_{t-1} + (dDO/dt) \times dt \quad (1)$$

where: DO_t is the concentration of DO in the water at time t in mg/L; DO_{t-1} is the concentration of DO in the water at time $t - 1$ in mg/L; and dDO/dt is the rate of change of DO in the water per hour in mg/L-h.

The DO carried by a water body is affected by both replenishment and consumption and thus depends on a number of influencing factors, including photosynthesis of the primary producers(P), aeration of the surface water(J), respiration in

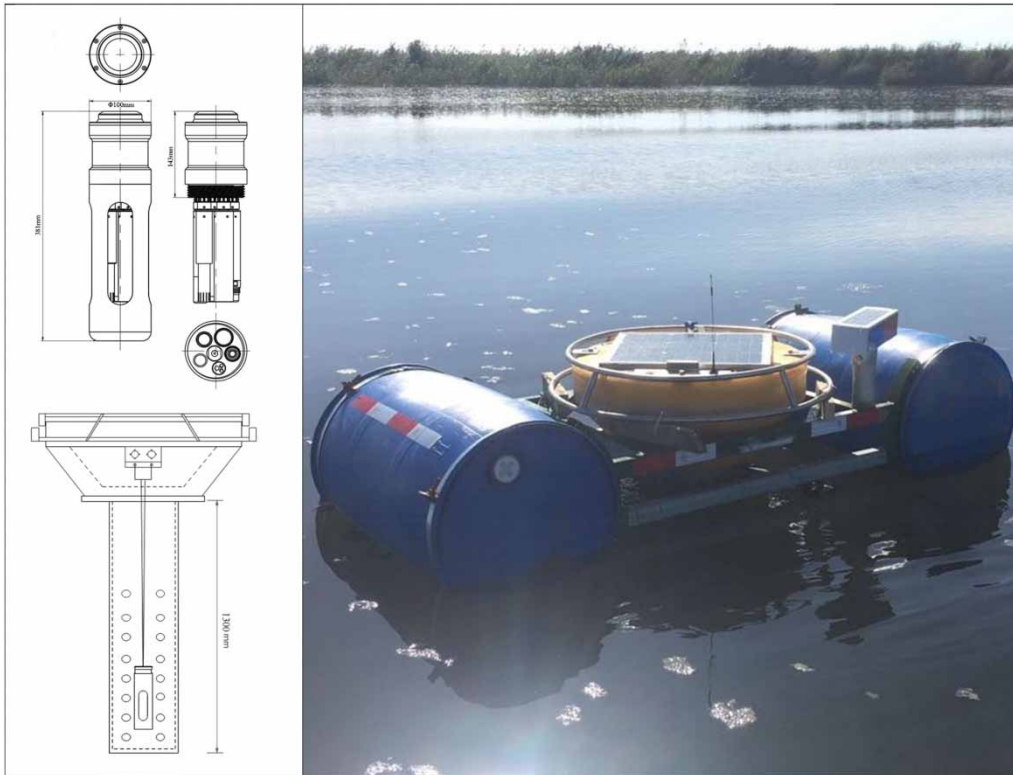


Figure 2 | Yosemite water quality multi-parameter sensor and buoy used for the online water quality monitoring.

water column(R), sediment or benthic organism oxygen consumption(S_{SOD}). This is expressed by the following equilibrium equation:

$$dDO/dt = P + J - R - S_{SOD} + C_{io} \quad (2)$$

where: dDO/dt is the hourly rate of change in the DO concentration and C_{io} is the difference value between the concentration of DO in the lake inflow and outflow water. All terms in the equation are in units of mg/L·h. The definition and calculation of specific parameters in the model are described below.

3.1.1. Oxygen production by photosynthesis

Photosynthesis is affected by factors such as water temperature, chlorophyll-a concentration (Chl-a), and photosynthetically active radiation(PAR). A one-dimensional equation derived from the Steele equation was used for calculating photosynthetic oxygen production based on the concentration of chlorophyll-a and PAR (Steele 1962) as follows:

$$P = P_c \times Chl-a \quad (3)$$

$$P_c = (\alpha_{par} \times R_s) \times P_{max} \times e^{(1-\alpha_{par} \times R_s)} \quad (4)$$

where P_c is the rate of oxygen production per units of Chl-a in mg/L·h and Chl-a is the measured chlorophyll-a concentration in the water body in mg/L. R_s is the solar radiation intensity in kW/m² and α_{par} is the ratio of the PAR to the solar radiation intensity in the study area in m²/kW, which is normally treated as a proportional constant in the calculation (Alados *et al.* 1996). P_{max} is the maximum oxygen production rate of photosynthesis under saturated light conditions in mg/L·h, which is dependent on temperature (T , °C) according to the Arrhenius equation and the following equation was applied (Megard

et al. 1984):

$$P_{\max} = 9.6 \times 1.306^{(T-20)} \quad (5)$$

As the Arrhenius equation for the temperature dependence of reaction rates (Megard *et al.* 1984) indicates that the oxygen production rate can be regarded as a dependent variable of temperature. In addition, the concentration of chlorophyll-a directly reflects the biomass of phytoplankton in the water body and indirectly reflects the nutrient content of the water body (Hoyer *et al.* 2002; Jiang *et al.* 2019).

3.1.2. Oxygen transfer by aeration

Aeration transfers oxygen across the water atmosphere interface and the direction oxygen moves depends on the saturation level of the DO in the water ($C_{sat} - C_s$). The rate of change in DO by aeration depends on the gas transfer velocity (K_L) at the air-water interface, which is dependent on water side turbulence and is often modeled as a function of wind speed. According to Gelda *et al.* (1996), the aeration of a water body can be estimated by:

$$J = \alpha_j \times (KL/H) \times (C_{sat} - C_s) \quad (6)$$

where: α_j is the oxygen production adjustment coefficient of aeration, which is dimensionless; K_L is the gas transfer velocity of the oxygen molecules in cm/h; H is the thickness of the surface layer in cm, which in the shallow lake in this study was set to 95 cm; C_{sat} is the concentration of the saturated DO in water at different temperatures in mg/L; and C_s is the actual measured value of the DO concentration in the water body in mg/L.

According to Crusius & Wanninkhof (2003), the migration coefficient for oxygen molecules over water at low wind speeds under wind conditions similar to those in the study area can be calculated as follows:

$$\text{when: } U < 3.7\text{m/s, } KL = 0.72U \quad (7)$$

$$\text{when: } U \geq 3.7\text{m/s, } KL = 4.33U - 13.3 \quad (8)$$

where: U is the wind speed measured at 10 m above the surface of the lake in m/s.

According to the 'Technical Guidelines for Environmental Impact Assessment' (HJ/T 2.3-1993) the formula for calculating saturated DO concentration in water bodies is:

$$C_{sat} = \frac{468}{(31.6 + T)} \quad (9)$$

where: T is the water temperature in °C.

3.1.3. Oxygen consumption by respiration

In eutrophic lakes, phytoplankton and zooplankton consumes DO in the water through respiration, reducing oxygen levels in the water. The equation derived by Hull *et al.* (2008) treats the water column respiration of phytoplankton as an approximately first-order kinetic equation, arguing that it primarily depends on the water temperature and chlorophyll-a content:

$$R = \alpha_r \times \theta_r^{(T-20)} \times Chl-a \quad (10)$$

where: α_r is the respiratory adjustment coefficient per hour; θ_r is a dimensionless temperature adjustment coefficient. In earlier research on this topic, Ambrose (1988) utilized a temperature coefficient of 1.045 and achieved a good fit for their eutrophication model calculations, so in this study we also opted to set the value of θ_r to 1.045.

3.1.4. Sediment oxygen consumption

As for the oxygen consumption of sediment, one is the rate at which oxygen from the water diffuses into the sediment is consumed, another is the rate at which reduced organic matter in the sediment is transported to the water body and then oxidized (Martin & Bella 1971). Ogunrombi & Dobbins (1970) found that the BOD that diffused back into the overlying water was 28

percent as large as the oxygen demand caused by oxygen diffusing into the benthic deposits. Some investigators believe that few studies have applied benthic demand is to DO mass equilibrium (Zison 1978). Therefore, in the study, the oxygen consumption of sediment and benthic organism was mainly considered as dissolved oxygen in the sediment invading the bottom of the lake.

The aerobic decomposition of organic matter by benthic organisms in the sediment consumes a large amount of DO and as this mainly occurs on the surface of the sediment, it is related to the water temperature, although it also depends on the physical, chemical, and biological properties of the lake bed (Zison 1978). The oxygen consumption equation of these lake sediments can be calculated as (Thomann & Mueller 1987):

$$S_{SOD} = S_{S20} \times \theta_s^{(T-20)} / Z \quad (11)$$

where: S_{S20} is the oxygen consumption of the sediment at a water temperature of 20 °C in mg/m²·h; Z is the overlying water depth in m , with the actual measured value in each of the study months falling in the range 1.89–1.93 m ; θ_s is the temperature adjustment coefficient, which is dimensionless. Zison (1978) reported the value of θ_s to be 1.07.

3.1.5. Change in DO due to transport by inflow and outflow

Drainage lakes have both sources of water inflow and outflow pathways, and the DO contained in the inflow and outflow water is a non-negligible factor that influences the dynamic properties of the DO in the lakes (Hudson & Vandergucht 2015). Ulansuhai Lake is a typical drainage lake in terms of water source type, which mainly from domestic sewage, industrial wastewater and farmland runoff in the Hetao Irrigation District, and hence its water quality is greatly affected by human activities (Yu *et al.* 2007). Unlike the supply water sources of most drainage lakes, the water replenished to the lake from the irrigation area carries a large amount of nitrogen and phosphorus nutrients, which is a major reason for the eutrophication of Ulansuhai Lake and at the same time, and the lake is also replenished with supersaturated DO, which is often present in water bodies (Sun *et al.* 2009; Quan *et al.* 2020). Extensive investigations have shown that the concentration of DO in the water bodies that inflow the lakes in the study area is generally higher than that in the outflow water (Jiang *et al.* 2019), and the difference between the DO levels in the two is an important determinant of the conditions of the DO in the water bodies in the study area. Therefore we assumed that the difference between the concentration of DO in the lake's supplementary water and that in the drainage remains approximately constant, with a value of C_{io} in mg/L·h, and this constant term C_{io} is used as a calibration parameter in the model to quantify the influence of the inflow and outflow water bodies on the DO levels in the lake.

For the purposes of this study, combining all the oxygen production and consumption equations in Formula 1 and 2, the mass equilibrium equation based on the change of DO in Ulansuhai Lake can be constructed. Because the model in this study is one-dimensional and the water depth of the lake is relatively shallow, it is assumed that the water is well mixed vertically.

3.2. DO model analysis

3.2.1. Model calibration and verification

During the modeling process, five parameters α_{par} , α_j , α_r , S_{S20} , and C_{io} were defined as the calibration parameters of the model, which were used for the calibration of the DO model. For the model calibration, a particle swarm optimization algorithm was used to optimize the calibration parameters, with the optimized parameter values being utilized in the model to simulate the dynamic change process for the DO. Although the water quality data was collected from July 2020 to November 2020, some external factors beyond our control meant that there were some gaps in this data. The hourly data was collected and uploaded to the cloud as the average value within that hour; missing data was estimated by interpolation during the modeling process to maintain the continuity of the data. The data was divided into two parts, with one part being used to calibrate the model (August 25th–November 13th; 80 days), and the other to verify the model's performance (July 4th–August 20th; 43 days). The data collected on the day the instruments were set in place was not used for either calibration or verification to allow time for the equipment to come to stabilization and ensure the reliability of the data. For model runs where the simulated DO concentration dropped below 0 mg/L, the dissolved oxygen concentration value at that time point was set to 0 mg/L. The calibration model was run until the measured value and the value calculated by the model achieved the best fit.

3.2.2. Model uncertainty analysis

After calibration, the model was subjected to an uncertainty analysis to confirm its reliability and stability. For the analysis, the uncertainty of each parameter (α_{par} , α_j , α_r , S_{S20} , C_{io}) was set between 50 and 150% of the calibrated value and only a single parameter was allowed to change, with the other parameters being maintained at the calibrated value. One thousand values within the uncertainty were randomly selected as input for each model run, and the model's output consisted of 1,000 sets of simulated DO change rate results. The average and standard deviation of the 1,000 sets of DO change rates was then calculated and compared with the average of the measured DO change rates as follows:

$$\sigma = \sqrt{\frac{1}{n} \sum_{i=1}^n \left[\left(\frac{dDO}{dt} \right)_i - \left(\frac{dDO}{dt} \right)_m \right]^2} \quad (12)$$

where: $(dDO/dt)_i$ is the rate of change of the DO concentration in the first unit time after changing the parameter in mg/L·h; $(dDO/dt)_m$ is the overall mean value after changing the parameter in mg/L·h; and n is the total number of samples utilized in the calculation.

3.2.3. Sensitivity analysis of the model

In addition to the uncertainty analysis of the model, a sensitivity analysis was also conducted to explore the sensitivity of each parameter to the model. The same five parameters (α_{par} , α_j , α_r , S_{S20} , C_{io}) were used for this analysis, and once again the value of only one parameter was changed each time, with the other parameter values remaining unchanged. The sensitivity was calculated using the following formula:

$$\Delta \left(\frac{dDO}{dt} \right) (0\%) = \frac{\sum_{i=1}^n \left\{ \left[\left(\frac{dDO}{dt} \right)_i^j - \left(\frac{dDO}{dt} \right)_i^k \right] / \left(\frac{dDO}{dt} \right)_i^k \times 100 \right\}}{n} \quad (13)$$

where: $(dDO/dt)_i^j$ is the rate of change of the DO concentration per unit time calculated by the model after the i^{th} parameter is changed, in mg/L·h; $(dDO/dt)_i^k$ is the rate of change of the DO concentration per unit time calculated by the model when the i^{th} parameter is equal to the calibration value, in mg/L·h; and n is the total number of samples utilized in the calculation.

3.2.4. Model evaluation

Two methods were adopted for the model evaluation, one based on the determination coefficient (R^2), and the other on the Nash efficiency coefficient (NSE) (Carrier *et al.* 2016). The determination coefficient is the goodness of fit, which ranges from 0 to 1; the closer R^2 is to 1, the better the fit of the model. The Nash efficiency coefficient, which is often used to evaluate the quality of hydrological model simulation results, ranges from $-\infty$ to 1; greater than 0 indicates that the model is generally reliable and again the closer it is to 1, the better the credibility of the model. NSE is calculated as:

$$NSE = 1 - \left[\frac{\sum_{i=1}^n (DO_i^b - DO_i^c)^2}{\sum_{i=1}^n (DO_i^b - DO^m)^2} \right] \quad (14)$$

where: DO_i^b is the i measured DO concentration value in mg/L; DO_i^c is the i simulated DO concentration value in mg/L; DO^m is the average value of the measured DO concentration in mg/L; and n represents the total number of datapoints used for the calculation.

The *Matlab2016*, *Origin2018* and *Excel2007* software packages were used for the calculation and analyses.

3.3. Analysis of the simulation results

3.3.1. Model calibration

The simulation results revealed that the overall trend predicted by the model was roughly consistent with the actual trend measured for the DO levels, and the degree of fit between the rate of change of the dissolved oxygen and the part of extreme

values is generally better in simulation and measurement, as shown in Figure 3(a). However, the amplitude in the dynamic variation of the simulated DO for some time periods does not reflect the actual variation, even where the trends in the variation are relatively consistent (Figure 3(b)). However, the *NSE* value of the model after calibration of 0.218 means that the simulation results obtained using the model are approximately equal to the values actually observed, confirming that the simulation results are generally credible; the R^2 value after calibration of 0.623 also suggests that the two are closely related (Table 1).

3.3.2. Uncertainty analysis

The average values of the DO change rates calculated by changing the 5 calibration parameters (α_{par} , α_j , α_r , S_{S20} , C_{io}) were: 0.0051, 0.0067, 0.0068, 0.0068, and 0.0072, respectively, as shown in Table 2. And we can see, all 5 of these average values are close to the average value (0.0069 mg/L-h) of the DO change rate calculated without changing the calibration parameters. Examining the standard deviation for each parameter, the degree of dispersion of these parameters was also relatively small, with all being within the acceptable range. Overall, parameter S_{S20} exhibits the greatest uncertainty, and parameter α_r the smallest.

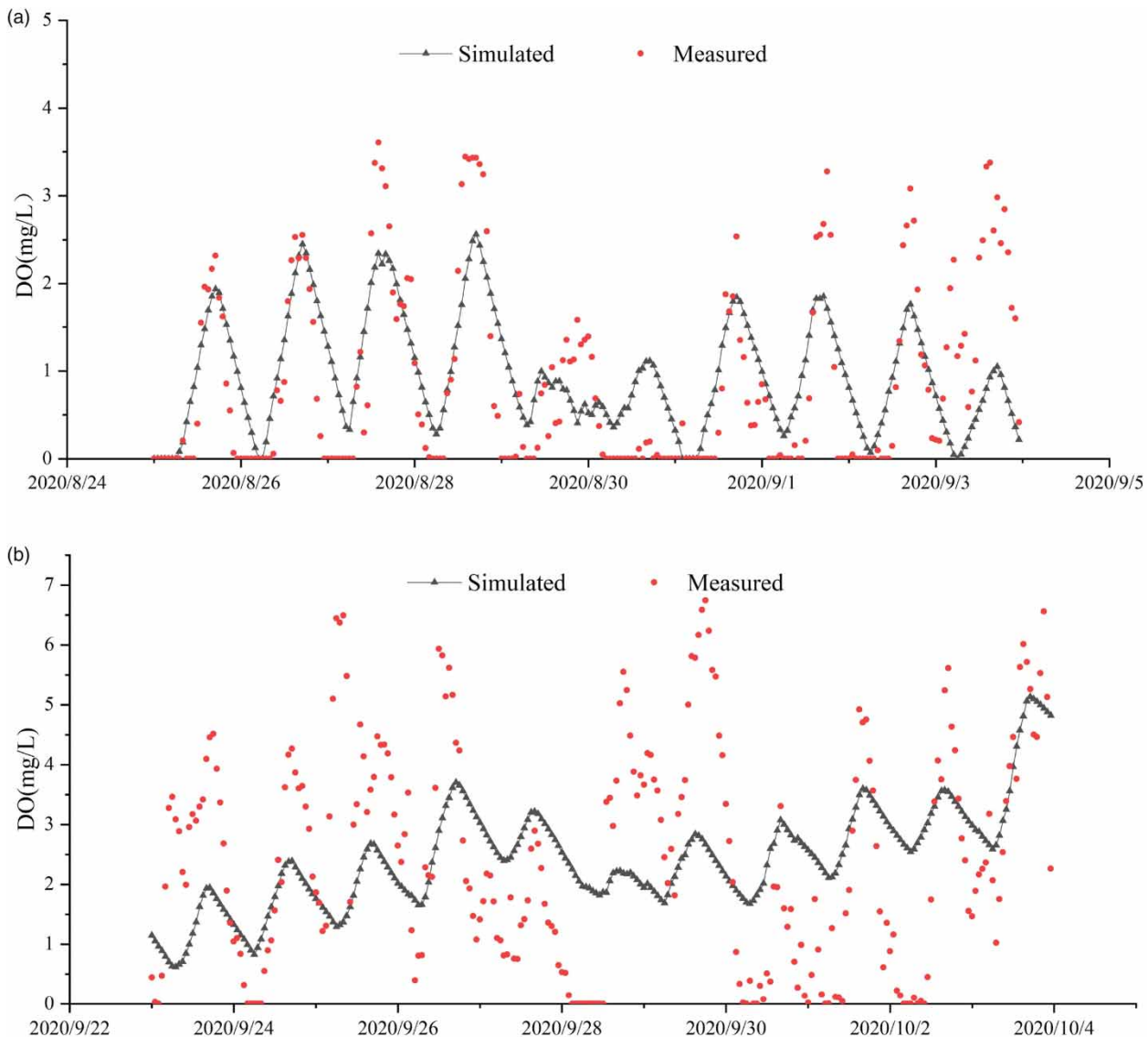


Figure 3 | Hourly change in DO concentration during the model calibration period: comparison of simulated and measured values.

Table 1 | Statistical results for the calibration and verification

Calibration			Verification		
<i>n</i>	<i>R</i> ²	<i>NSE</i>	<i>n</i>	<i>R</i> ²	<i>NSE</i>
1,944	0.623	0.218	977	0.419	0.305

Table 2 | Model calibration parameters and uncertainty analysis

Calibration parameters	Calibration value	Uncertainty analysis	
		Calibration value range	Average value (mg/L·h) ± standard deviation
$\alpha_{par}(m^2/kW)$	1.5821	[0.7911,2.3732]	0.0051 ± 1.53E-05
α_j	0.2083	[0.1042,0.3125]	0.0067 ± 2.61E-05
$\alpha_r(h^{-1})$	0.1275	[0.0638,0.1913]	0.0068 ± 2.38E-07
$S_{S20}(mg/m^2 \cdot h)$	0.4042	[0.2021,0.6063]	0.0068 ± 9.10E-04
$C_{io}(mg/L \cdot h)$	0.0660	[0.0330,0.0990]	0.0072 ± 1.84E-04

3.3.3. Sensitivity analysis

The data presented in Table 3 shows that throughout the entire calibration period, the DO dynamic model is most sensitive to the oxygen consumption coefficient of the sediment (S_{S20}), slightly more sensitive to the difference value between the concentration of DO in the lake inflow and outflow water (C_{io}), and least sensitive to the respiration adjustment coefficient (α_r). The ratio of the photosynthetically active radiation to the solar radiation (α_{par}) is close to the sensitivity of the aeration adjustment coefficient (α_j). Parameter S_{S20} has the greatest influence on the model, with the other parameters exhibiting progressively less influence.

3.3.4. Model verification

Once the parameters had been calibrated and analyzed they were input into the model to analyze the time-by-time measurements for the remaining DO concentration data (July 4th–August 20th) and verify the model performance. Overall, the dynamic change in the simulated value is in good agreement with the dynamic change of the measured value most of the time, including the ‘cliff-edge’ drop in the DO concentration on July 22 shown in Figure 4(a). Although the model fails to accurately predict the amplitude of the change in DO concentration, this does not affect the consistency of the two dynamic changes, as shown in Figure 4(b). According to the evaluation results of the model, the *NSE* value of the verification result is 0.305, and the R^2 value is 0.419, confirming that the simulation values for the DO concentration during the verification period, shown in Figure 4, are generally credible.

4. DO EQUILIBRIUM ANALYSIS

4.1. Analysis of trends in *P*, *J*, *R*, and S_{SOD}

Once the calibration and verification had been successfully completed, a box plot of the per unit time simulated values for a 24-hour period was analyzed to examine the overall trends in oxygen production and consumption over the course of the day

Table 3 | Model sensitivity analysis

Calibration parameters	Calibration value for max	Calibration value for min	$\Delta(dDO/dt)\%$ for max	$\Delta(dDO/dt)\%$ for min
$\alpha_{par}(m^2/kW)$	2.3732	0.7911	−18.0219	8.6337
α_j	0.3125	0.1024	−12.9267	12.9267
$\alpha_r(h^{-1})$	0.1913	0.0638	2.3543	−2.3543
$S_{S20}(mg/m^2 \cdot h)$	0.6063	0.2021	120.6319	−120.6319
$C_{io}(mg/L \cdot h)$	0.0990	0.0330	−62.0314	62.0314

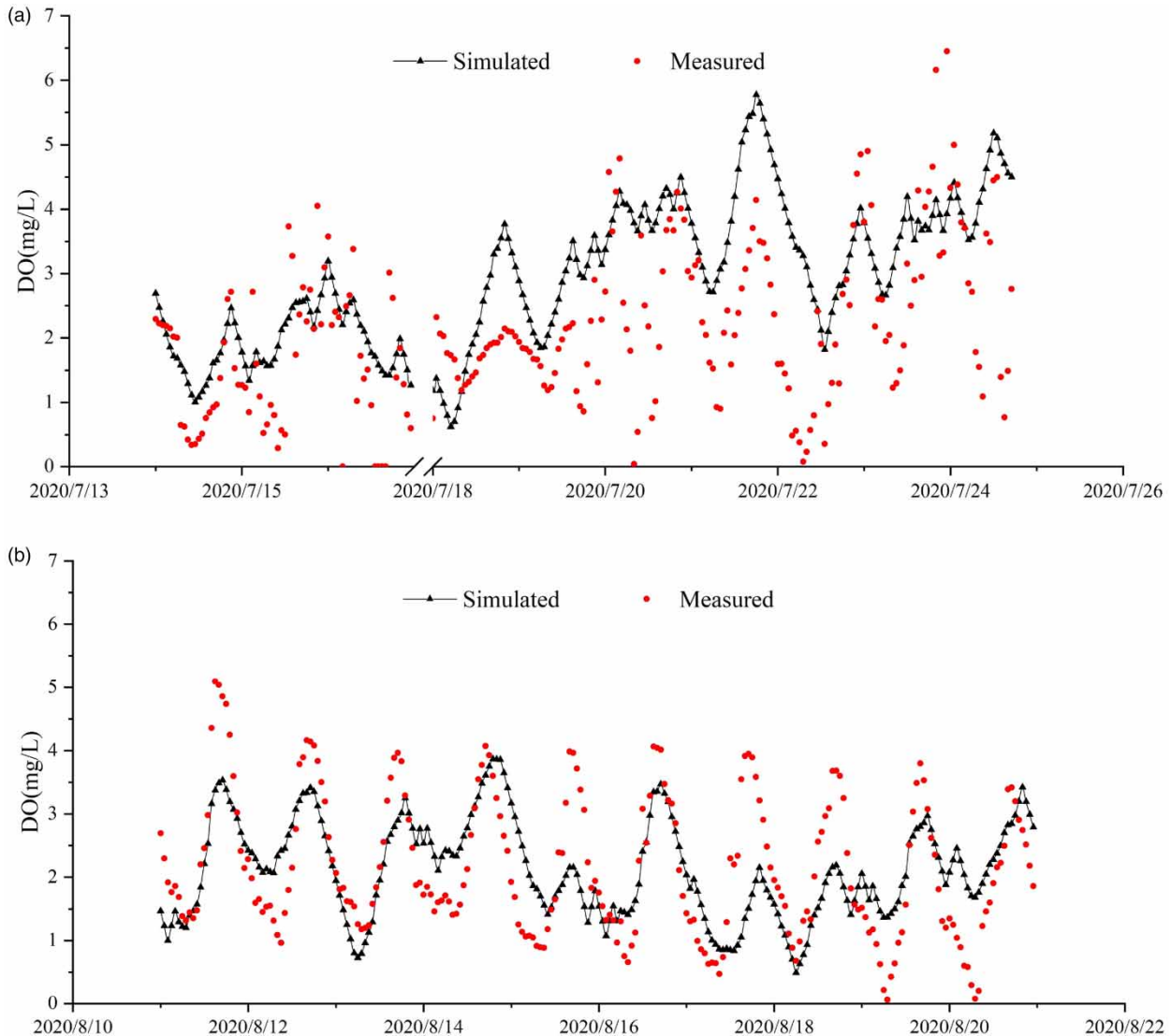


Figure 4 | Hourly changes in the dissolved oxygen concentration during the model verification period: Comparison of simulated and measured values.

(Figure 5(a)). The photosynthetic oxygen production generally starts at 5 in the morning and follows a clear upward trend with increasing daytime solar radiation. The average oxygen production rate rises from 5.86×10^{-5} mg/L·h at 5 a.m. to a midday peak of 0.22 mg/L·h, after which it decreases gradually during the afternoon, reaching a level of 6.66×10^{-5} mg/L·h at 7 p.m., when darkness falls. The overall pattern in the oxygen production is thus highly consistent with the duration of solar radiation. During the night-time hours the lack of solar radiation, its main driving force, means that the oxygen produced through photosynthesis is 0 mg/L·h approximately, hence photosynthesis does not contribute to any overnight changes in the lake's DO levels.

There were no obvious patterns in the amount of aeration oxygen produced. The oxygen production levels shown in Figure 5(b) indicate that the oxygen production due to aeration fluctuates very little across the 24-hour simulation period. The inherent uncertainty in environmental factors such as the instantaneous wind speed, which can vary considerably over very short periods of time, will inevitably lead to some abnormal values of oxygen production, but overall the degree of dispersion in the oxygen production data is relatively small and the differences in the levels of oxygen production for different periods tend to be low. The oxygen production in each period essentially follows a chi-square distribution, with the outliers generally appearing on the high side so the distribution exhibits a right skew with a heavier tail; and the degree of

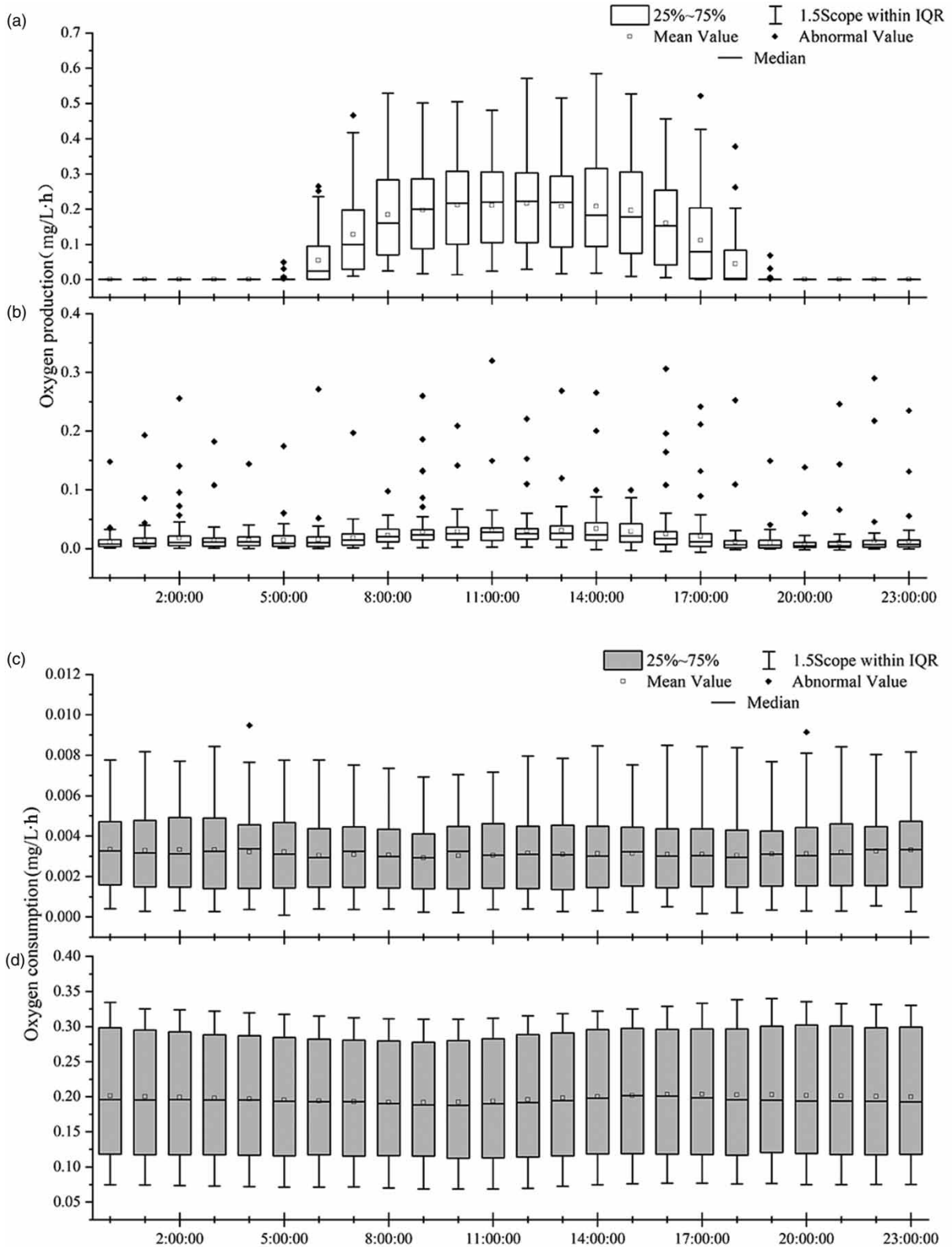


Figure 5 | 24-hour box diagram of changes in the oxygen production of photosynthesis (a), aeration (b) and the oxygen consumption of respiration (c), sediment (d).

freedom is small. Overall, the aeration rate is effectively maintained at about 0.3 mg/L·h, where the average peak value appears at 1 p.m., when the oxygen production rate is about 0.05 mg/L·h, and the average valley value at midnight, when the oxygen production rate is about 0.02 mg/L·h.

Relative to the uncertainty associated with the effect of external environmental factors on oxygen production, the dataset collected for this study shows that the oxygen consumption due to respiration and sediment are mainly affected by environmental factors within the body of water itself. The average oxygen consumption of the respiration remained stable across the 24-hours period, exhibiting no significant changes (Figure 5(c)). The median of the oxygen consumption in the simulated data is basically consistent with the average oxygen consumption, and exhibiting the characteristics of a standard normal distribution with just a few outliers. The average oxygen consumption rate due to respiration appears to follow no regular pattern and its maximum is only slightly different from the minimum. The average oxygen consumption rate across the 24 hour period is 3.15×10^{-3} mg/L·h; the peak value of the average oxygen consumption rate of 3.33×10^{-3} mg/L·h occurs at midnight and valley value, at 2.92×10^{-3} mg/L·h, occurs at 9 a.m.

The average oxygen consumption per unit time in the sediment follows a similar trend to that seen for respiration (Figure 5(d)). It is relatively stable, but the degree of dispersion of the oxygen consumption rate across a single period is relatively discrete. On the whole, the skewness of the oxygen consumption rate of the sediment is relatively weak and the distribution is generally normal, with no outliers. The range in the variation in the average oxygen consumption rate of the sediment is basically less than 0.01 mg/L·h, although this does change irregularly. The highest point in the peak value for the sediment oxygen consumption rate is at 5 p.m., at which point the oxygen consumption rate is 0.20 mg/L·h; the lowest point in the oxygen consumption rate appears at 9 a.m., with an oxygen consumption rate of 0.19 mg/L·h.

4.2. Analysis of the cumulative change in P , J , R , and S_{SOD}

Drawing a cumulative curve allows us to objectively reflect changes in the trends of both oxygen production and consumption over time, highlighting the key nodes of sudden changes. The accumulation of time series were created and plotted, showing the cumulative effect of these changes in oxygen production and consumption across the study period. As the Figure 6 shows, photosynthesis, respiration, and sediment drive long-term changes in oxygen production and consumption, with the initial, fairly uniform, upward trend in July, August and September only slowing once the weather began to turn cold around mid-October. The oxygen production due to aeration also showed a generally upward trend, albeit with a number of inflection points where a sudden sharp increase is followed by a return to earlier levels. For example, from August 11th to 12th, the oxygen production rate jumps from 6.63×10^{-5} mg/L·h to 0.43 mg/L·h,

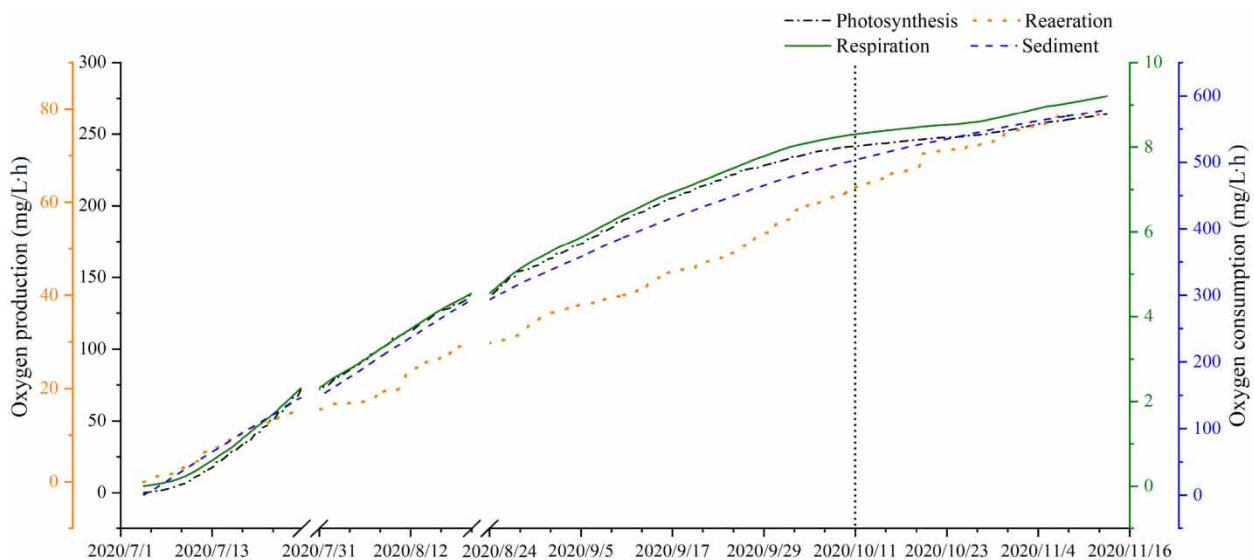


Figure 6 | The cumulative change in the oxygen production of photosynthetic (black), aeration (orange) and the oxygen consumption of respiration (green), sediment (blue).

in a very short period of time. It then remains unchanged for several days before resuming its upward trend. On October 20th, this happens again, rising rapidly from 0.02 mg/L-h to 0.42 mg/L-h then, gradually decreasing. These changes are likely due to the influence of uncertainties in the natural environment, especially changes in wind speed. However, no matter which driving factor, all of them jointly drive the DO to equilibrium in the simulation of the change.

4.3. Analysis of the proportion of DO supplementation and consumption

In general, in terms of the reoxygenation of lake water bodies, the effects of photosynthesis and aeration far outweigh the other factors involved. The average oxygen production apportionment between photosynthesis and aeration for each 24 hour interval during the study period was therefore analyzed without taking into account the other factors influencing the dissolved oxygen levels as shown in Figure 7(a). The contribution of photosynthetic oxygen production is generally lower than 6% before sunrise, reaching its nadir of 4.20% at 2 a.m. After sunrise, as the solar radiation intensity increases, the photosynthetic oxygen production rises quickly, reaching a maximum of 85.80% of the total at 8 a.m. The pattern in the proportion of oxygen produced by aeration is the mirror image of that for photosynthesis, with the highest contribution of 95.80% and the lowest of 14.20% occurring at 2 a.m. and 8 a.m., respectively.

Compared with the regular changes in oxygen production, which are strongly affected by environmental factors, the pattern for oxygen consumption through respiration and sediment oxygen consumption is relatively stable. The average apportionment of respiration and sediment oxygen consumption over a 24-hour period is shown in Figure 7(b). The oxygen consumption in the sediment is the predominant factor, consistently staying at levels of over 98% of the total. This is because the oxygen consumption in sediments does not change significantly without an additional contribution from the external environment or human factors. Here, the largest proportion was 98.56%, at 6 p.m., and the smallest was 98.41%, at 2 a.m.. The pattern in the oxygen consumption due to respiration was again a mirror image of that for sediment consumption, with the largest proportion of 1.59% and the smallest of 1.44% appearing at 2 a.m. and 6 p.m., respectively.

The proportion of total oxygen production and oxygen consumption of each driving factor is represented by pie chart, as shown in Figure 8. Looking at the contribution of oxygen production (Figure 8(a)), photosynthesis and supplementary water of DO account for more than 80% of the total oxygen production in the lake. The largest contribution came from photosynthesis, which was responsible for 49.28% of the oxygen production, but supplementary water and drainage was also a major contributor, at 36%. Aeration of the water body accounted for only 14.72% of the lake's oxygen production.

In terms of oxygen consumption in eutrophic bodies of water, the aerobic decomposition of sediment is largely responsible for the oxygen consumption. As the analysis shows (Figure 8(b)), oxygen consumption in the sediment accounted for more than 98% of the total, with the remaining 1.56% being consumed by respiration. This clearly shows that oxygen take-up by sediment in shallow-water eutrophic lakes is the primary factor driving oxygen consumption in water bodies. These results clearly show that for Ulansuhai Lake and other lakes of the same type during the non-frozen period, oxygen from

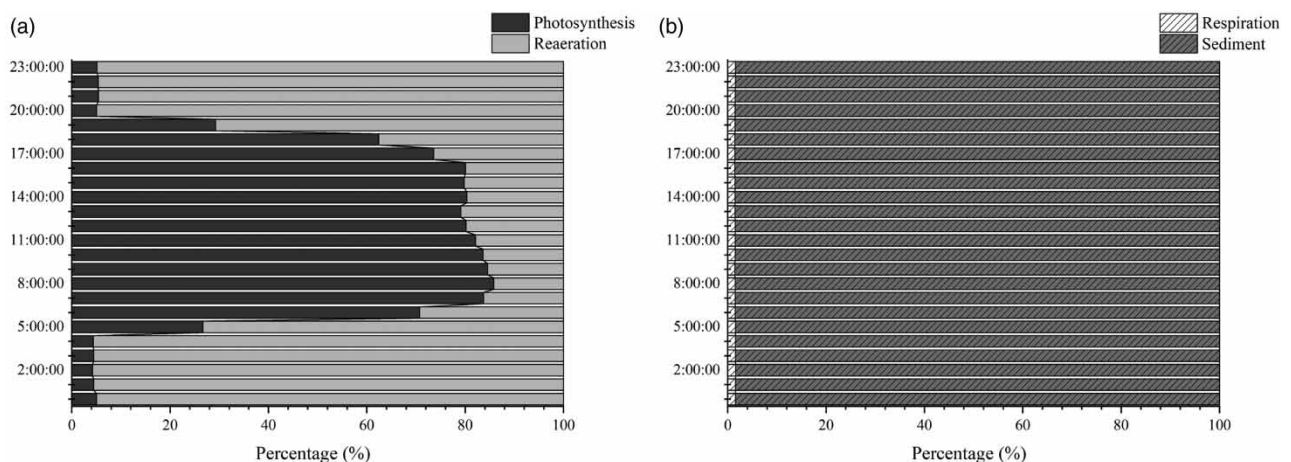


Figure 7 | The relative contribution rate of photosynthesis and aeration for oxygen production (a), the relative contribution rate of respiration and sediment for oxygen consumption (b).

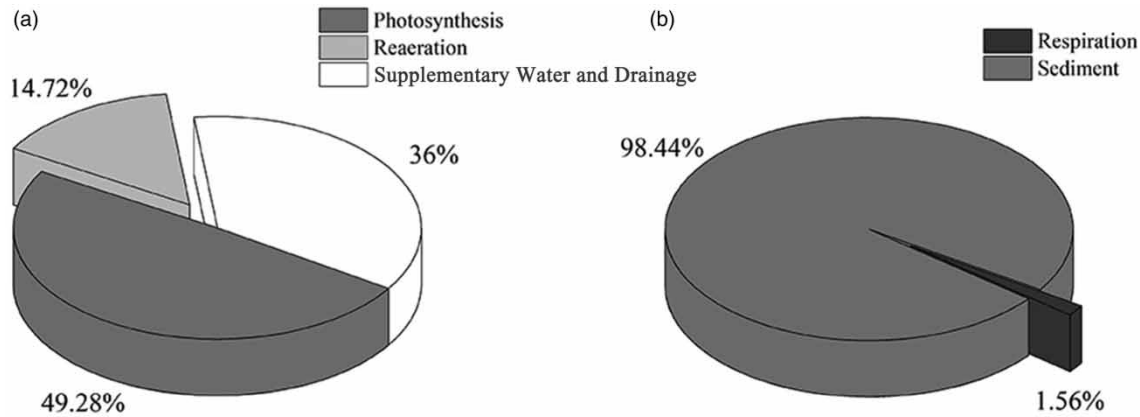


Figure 8 | The cumulative contribution of photosynthesis, aeration, and the amount of oxygen carried by supplementary water and drainage (a) to the oxygen production, as well as the cumulative contribution of respiration and sediment to the oxygen consumption (b).

photosynthesis and oxygen consumption by sediment are the most crucial factors that determine the dynamic balance of DO in the lake water.

4.4. Meteorological factors and the interaction between water temperature and DO

Solar radiation and wind speed are the two main forces driving lake reoxygenation. The amount of oxygen produced each hour in photosynthesis rises and falls parallel with changes in solar radiation, which is clearly shown in the overall daily patterns found in the data (Figure 9(a)). However, variations in the oxygen production levels did not consistently track changes in the solar radiation. For example, the maximum solar radiation on September 10th was 790.6 W/m^2 and the maximum oxygen production rate during photosynthesis on the same day was 0.37 mg/L-h , but although the maximum solar radiation the following day was much higher, at 878.1 W/m^2 , the maximum oxygen production rate during photosynthesis was only 0.29 mg/L-h .

At the air-water interface, where aeration occurs, changes in wind speed largely determine the amount of oxygen entering the water body or released to the atmosphere. The results shown in Figure 9(b) support this conclusion. When the DO content in a water body is below the saturation point, higher wind speeds will accelerate the transfer of atmospheric oxygen into the water; once the DO in the water body reaches saturation the process is reversed, with higher wind speeds instead transferring any excess oxygen to the atmosphere. In the latter part of the study period, supersaturation of DO in the lake water was observed in 1.44% of the readings collected, so oxygen could be spilling out of the water.

Water temperature indirectly affects the concentration of DO by affecting the biomass, species, and activity of aquatic plants, phytoplankton, zooplankton, and microorganism. Then it can also directly affect the concentration of dissolved oxygen by limiting the saturation of the water. Whether directly or indirectly, the water temperature plays a pivotal role in both the reoxygenation and oxygen consumption processes, which having a significant effect on the level of dissolved oxygen. The results of the correlation analysis conducted for this study showed that reveal a high positive correlation between water temperature and both respiration and sediment in Figure 10. It represents that the oxygen production rates photosynthesis, the oxygen consumption rates of respiration and sediment all become more productive and rise as the water temperature rises. However, the correlation between water temperature and photosynthesis is weak and even close to irrelevant to aeration. It can be concluded that water temperature plays a more significant role in the process of oxygen consumption.

5. DISCUSSION

The oxygen consumption in the sediment was found to be the most sensitive to the model, while that of water column respiration was the weakest. In summer and autumn, a great deal of organic waste, including plankton biomass, feces, bait, and dead animals and plants are deposited at the bottom of the lake, and oxygen-consuming decomposition in the sediment is therefore very active (Woszczyk *et al.* 2011). After investigation, Ulansuhai Lake is a drainage lake in the Hetao Irrigation District, considerable amounts of exogenous pollutants have been deposited over the years, which coupled with the

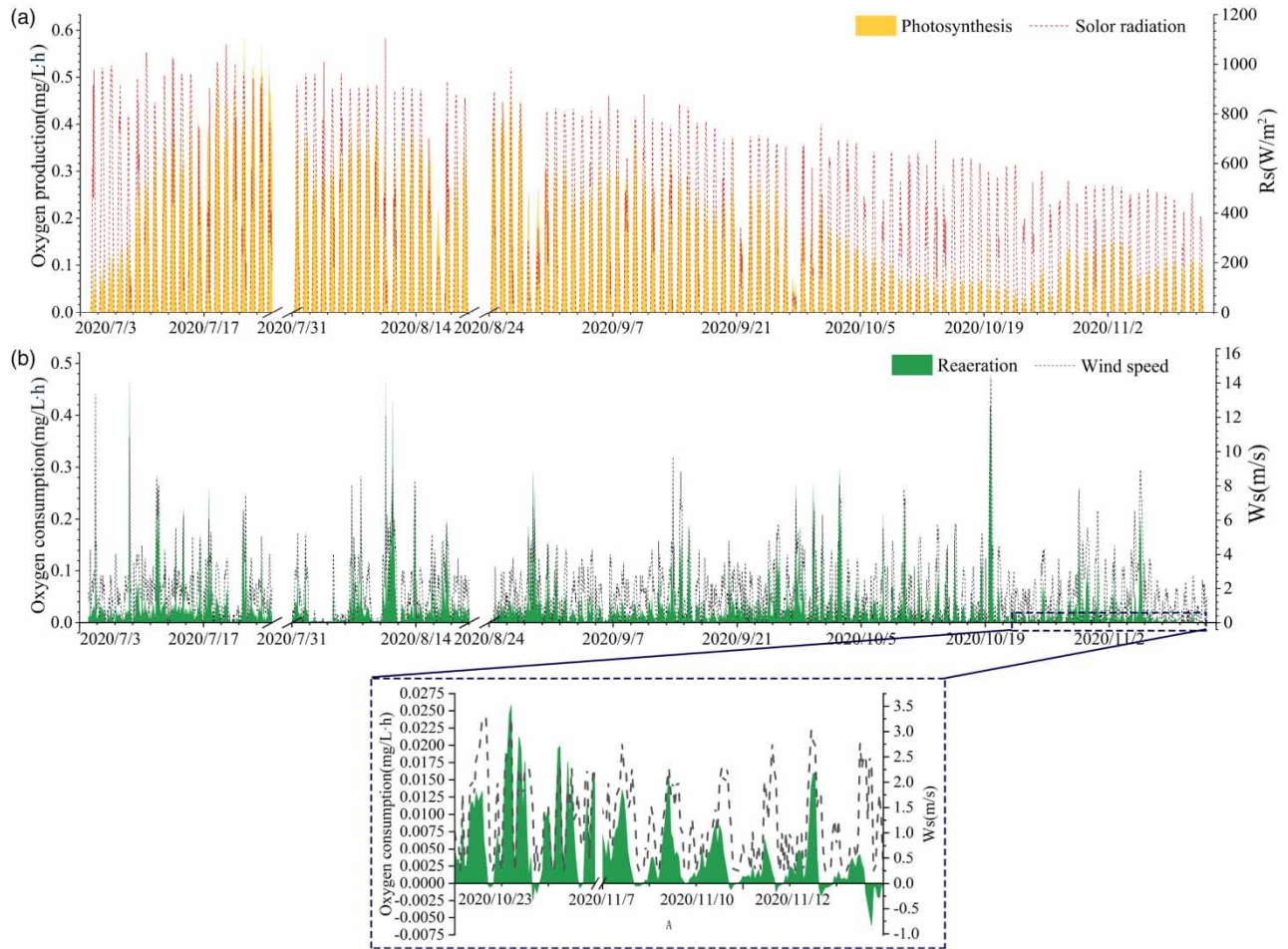


Figure 9 | Comparison of changes in the trends of photosynthetic oxygen production and solar radiation intensity (a), and aeration oxygen production and wind speed (b).

accumulation of aquatic plant residues (Zhu *et al.* 2017) have led to a serious concentration of organic matter in the lake's bottom mud. Unfortunately, in shallow lakes these sediments are prone to re-suspension due to the disturbance of wind and waves (Xu *et al.* 2018), raising their contribution to oxygen consumption in the lake water (Zhu *et al.* 2017). From the end of summer and early autumn to the end of autumn, the functional populations of the dominant phytoplankton in Ulansuhai Lake are thus greatly reduced (Li *et al.* 2015). At the same time, the solar radiation and water temperature are decreasing, which also inhibits the biological activities of phytoplankton and decreases the oxygen consumption due to respiration. All of these environmental conditions may cause great differences in the above drivers of oxygen consumption. In addition to its remarkable sensitivity, the oxygen consumption of sediment also dominates the study. With regard to this phenomenon, Baxa *et al.* (2021) found that in shallow water ecosystems such as those commonly found in fishponds, the oxygen demand in sediments under low chlorophyll-a concentrations accounts for 70–90% of the total demand. During the monitoring period, the chlorophyll-a concentration in Ulansuhai Lake was less than 100 $\mu\text{g/L}$, and the proportion of oxygen consumption in sediments obtained by the simulation calculation is thus consistent with the results reported by Baxa. In addition, the experimental results of Opaliński *et al.* (2010) in the Baltic Sea also showed that sediments and meiobenthos in the bottom were the major oxygen consumers in the shallow littoral, which oxygen consumption is over 80%.

The findings of our study reveal that the photosynthesis intensity does not in fact reach its peak value when the solar radiation intensity is at its highest. This is likely due to the underlying mechanisms governing the photorespiration of phytoplankton. Photorespiration usually occurs when photosynthetic cells in a high oxygen and low carbon dioxide environment are exposed to light (Busch 2013). Experimental studies (Hull *et al.* 2008) have shown that the primary production of lake water in summer decreases due to photorespiration when solar radiation reaches its peak. Photorespiration can

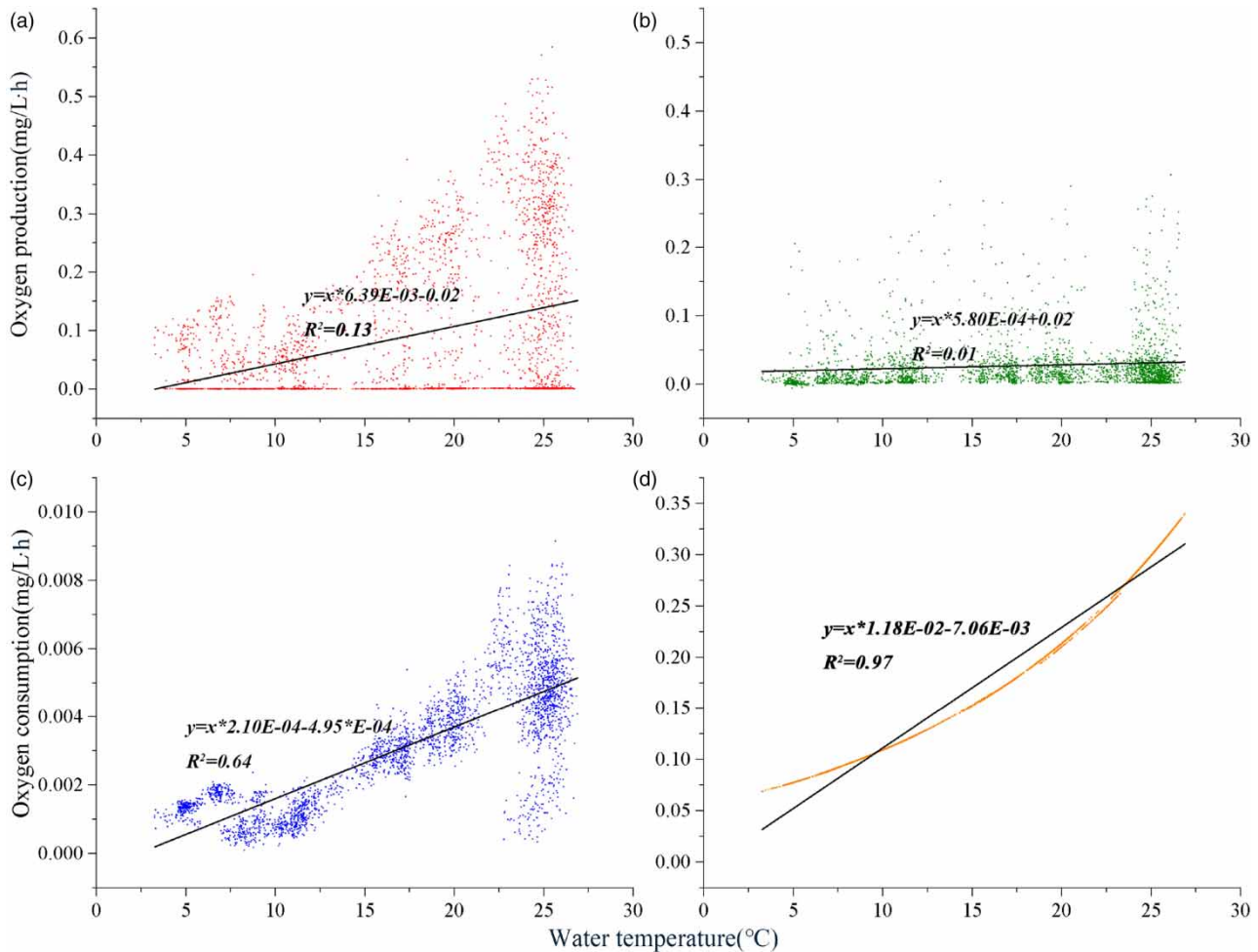


Figure 10 | Correlation between water temperature and photosynthesis (a), aeration (b), respiration (c), and sediment oxygen consumption (d).

significantly slow down photosynthesis, as it consumes the energy produced by photosynthesis. Moreover, the damage of photosynthetic pigments may take place under high PAR (Buma *et al.* 2006). This is a phenomenon that occurs frequently in phytoplankton in water bodies, and it leads directly to decreased photosynthetic performance. Therefore, the stronger the photorespiration leads the lower the photosynthetic productivity.

In the analysis of driving factors of oxygen production, photosynthesis is the main source of DO in lake water. This is a marked contrast with the oxygen production processes in rivers, especially those with fast water flow, where aeration is the main driving factor (Liu *et al.* 2005; Correa-González *et al.* 2014); these results confirm that in eutrophic still water lakes photosynthesis takes over as the main source of oxygen increase. Moreover, the data collected for the current study revealed that the water in Ulansuhai Lake experienced intermittent hypoxia and anaerobic episodes during the night-time in July and in at the end of August until the beginning of September. A comparative analysis of the factors driving these changes in the DO levels in the lake water during these periods revealed that the increase in the dissolved oxygen levels due to the supplementary water and the aeration were insufficient to maintain the balance with the oxygen consumption of the lake at night, when there was no oxygenation due to photosynthesis. Therefore, this proves that the change of dissolved oxygen will therefore tend to weaken or even stagnate over time. In addition, supersaturation of DO is also much more likely to occur towards the end of autumn. There were several times of DO supersaturation during the daytime from October 22th to 24th and November 8th to 13th of the study period, it directly results in the negative value of aeration calculated by the simulation (Figure 9(b)). This phenomenon indicates that aeration does not affect the level of DO in the water during this period. However, it also cannot be ruled out whether DO in water escapes into the air.

The simulation calculations revealed that the model sometimes was unable to deliver accurate predictions when dealing with sudden and occasional oxygen deficit situations, which may affect the reliability of efforts to identify the factors driving major changes in the level of DO in the lake water. In cold and arid areas such as Ulansuhai Lake, as the lake water temperature drops the accuracy of the model also gradually becomes unstable. Therefore, for lakes in cold and arid regions, it is necessary to extend this research to establish a separate dynamic model that describes how the DO changes during the freezing period to simulate and predict DO levels and support the scientific management and protection of shallow eutrophic lakes like Ulansuhai Lake.

6. CONCLUSIONS

A deterministic model of DO combined with the environmental characteristics of the study area was improved, then the DO data during the study period were simulated, calibrated, and validated. The determination coefficients of calibration and validation results of the model were 0.623 and 0.419, respectively. Nash efficiency coefficients are 0.218 and 0.305, respectively. It shows that the simulation results of the model are generally reliable.

In further analysis of the simulation results of the model, the change trend of the average oxygen production and consumption rate per unit time in 24 hours. The maximum oxygen production rate of photosynthesis was 0.22 mg/L·h, and the lowest oxygen production rate was close to 0 mg/L·h in the absence of light. The maximum and minimum oxygen production rates of aeration were 0.05 mg/L·h and 0.02 mg/L·h, respectively. The maximum and minimum respiration rates were 3.33×10^{-3} mg/L·h and 2.92×10^{-3} mg/L·h, respectively. The maximum and minimum oxygen consumption rates of sediments were 0.20 mg/L·h and 0.19 mg/L·h, respectively.

During the research period of more than four months, the main source of DO in Ulansuhai Lake was oxygen production by photosynthesis, accounting for 49.28% of the total. The second was DO carried by lake supplementary water and drainage, accounting for 36%. The oxygen production ratio of surface aeration only was 14.72%. Almost all of the oxygen consumption in the lake water was in the layer of sediments, which accounted for 98.44% of the total. The aerobic respiration of water accounted for the remaining 1.56%.

In addition, in the interaction analysis established with environmental factors, it is found that the overall relationship between solar radiation intensity and photosynthesis as well as wind speed and aeration is consistent. However, there is still a certain degree of uncertainty in the simulation of photosynthetic oxygen sources by radiation intensity. The analysis results of water temperature and respiration, sediment oxygen consumption showed a significant positive correlation, which proved that water temperature plays an important role in driving the consumption of DO.

DATA AVAILABILITY STATEMENT

All relevant data are included in the paper or its Supplementary Information.

REFERENCES

- Alados, I., Foyo-Moreno, I. Y. & Alados-Arboledas, L. 1996 Photosynthetically active radiation: measurements and modelling. *Agricultural and Forest Meteorology* **78** (1–2), 121–131.
- Ambrose, R. B. 1988 *WASP4, A Hydrodynamic and Water Quality Model: Model Theory, User's Manual and Programmer's Guide*. Environmental Research Laboratory, United States.
- Baxa, M., Musil, M., Kummel, M., Hanzlík, P., Tesařová, B. & Pechar, L. 2021 Dissolved oxygen deficits in a shallow eutrophic aquatic ecosystem (fishpond)—Sediment oxygen demand and water column respiration alternately drive the oxygen regime. *Science of The Total Environment* **766**, 142647.
- Buma, A. G., Wright, S. W., van den Enden, R., van de Poll, W. H. & Davidson, A. T. 2006 PAR acclimation and UVBR-induced DNA damage in Antarctic marine microalgae. *Marine Ecology Progress Series* **315**, 33–42.
- Busch, F. A. 2013 Current methods for estimating the rate of photorespiration in leaves. *Plant Biology* **15** (4), 648–655.
- Carrier, C. A., Kalra, A. & Ahmad, S. 2016 Long-range precipitation forecasts using paleoclimate reconstructions in the western United States. *Journal of Mountain Science* **13** (4), 614–632.
- Chapra, S. C. & Di Toro, D. M. 1991 Delta method for estimating primary production, respiration, and reaeration in streams. *Journal of Environmental Engineering* **117** (5), 640–655.
- Chinyama, A., Ncube, R. & Ela, W. 2016 Critical pollution levels in Umguza River, Zimbabwe. *Physics and Chemistry of the Earth, Parts A/B/C* **93**, 76–83.
- Correa-González, J. C., del Carmen Chávez-Parga, M., Cortés, J. A. & Pérez-Munguía, R. M. 2014 Photosynthesis, respiration and reaeration in a stream with complex dissolved oxygen pattern and temperature dependence. *Ecological Modeling* **273**, 220–227.

- Crusius, J. & Wanninkhof, R. 2003 Gas transfer velocities measured at low wind speed over a lake. *Limnology and Oceanography* **48** (3), 1010–1017.
- Gelda, R. K., Auer, M. T., Effler, S. W., Chapra, S. C. & Storey, M. L. 1996 Determination of reaeration coefficients: whole-lake approach. *Journal of Environmental Engineering* **122** (4), 269–275.
- HJ/T 2.3-1993 1993 *Technical Guidelines for Environmental Impact Assessment. Surface Water Environment*. Industry standard – Environmental protection of the People's Republic of China.
- Houser, J. N., Bartsch, L. A., Richardson, W. B., Rogala, J. T. & Sullivan, J. F. 2015 Ecosystem metabolism and nutrient dynamics in the main channel and backwaters of the Upper Mississippi River. *Freshwater Biology* **60** (9), 1863–1879.
- Hoyer, M. V., Frazer, T. K., Notestein, S. K. & Canfield Jr, D. E. 2002 Nutrient, chlorophyll, and water clarity relationships in Florida's nearshore coastal waters with comparisons to freshwater lakes. *Canadian Journal of Fisheries and Aquatic Sciences* **59** (6), 1024–1031.
- Huang, Y. Q., Cai, D. S., Li, M. Q., Wu, T. H., Wu, P. G. & Li, L. 2019 Influence of changes in dissolved oxygen content on fish behavioral trajectories during water eutrophication. *Applied Ecology and Environmental Research* **17** (1), 653–666.
- Hudson, J. J. & Vandergucht, D. M. 2015 Spatial and temporal patterns in physical properties and dissolved oxygen in Lake Diefenbaker, a large reservoir on the Canadian Prairies. *Journal of Great Lakes Research* **41**, 22–33.
- Hull, V., Parrella, L. & Falcucci, M. 2008 Modelling dissolved oxygen dynamics in coastal lagoons. *Ecological Modelling* **211** (3–4), 468–480.
- Jiang, X. Y., Li, C. Y., Shi, X. H., Sun, B., Zhao, S. N. & Sun, C. 2019 Spatial and temporal distribution of chlorophyll-a concentration and its relationships with environmental factors in Lake Ulansuhai. *Ecology and Environmental Sciences* **28** (5), 964–973.
- Li, X., Li, J. R., Xu, X. Q. & Bai, X. L. 2015 Seasonal succession of phytoplankton functional groups and their relationship with environmental factors in Ulansuhai Lake. *Ecology and Environmental Sciences* **24** (10), 1668–1675.
- Liu, H. Y., Qu, K. M. & Mao, S. S. 2005 Survey of both the variation and the absorption and consumption budget of dissolved oxygen in culture ponds. *Marine Fisheries Research* **26** (02), 79–84.
- Malve, O., Laine, M. & Haario, H. 2005 Estimation of winter respiration rates and prediction of oxygen regime in a lake using Bayesian inference. *Ecological Modelling* **182** (2), 183–197.
- Martin, D. C. & Bella, D. A. 1971 Effect of mixing on oxygen uptake rate of estuarine bottom deposits. *Journal (Water Pollution Control Federation)* **43** (9), 1865–1876.
- Megard, R. O., Tonkyn, D. W. & Senft, W. H. 1984 Kinetics of oxygenic photosynthesis in planktonic algae. *Journal of Plankton Research* **6** (2), 325–337.
- Murniati, E., Geissler, S. & Lorke, A. 2015 Short-term and seasonal variability of oxygen fluxes at the sediment–water interface in a riverine lake. *Aquatic Sciences* **77** (2), 183–196.
- Odum, H. T. 1956 Primary production in flowing waters 1. *Limnology and Oceanography* **1** (2), 102–117.
- Ogunrombi, J. A. & Dobbins, W. E. 1970 The effects of benthic deposits on the oxygen resources of natural streams. *Journal (Water Pollution Control Federation)* **42** (4), 538–552.
- Opaliński, K. W., Maciejewska, K., Urban-Malinga, B. & Węslawski, J. M. 2010 The oxygen fluxes of sandy littoral areas: quantifying primary and secondary producers in the Baltic Sea. *Marine Pollution Bulletin* **61** (4–6), 211–214.
- Parkhill, K. L. & Gulliver, J. S. 1999 Modeling the effect of light on whole-stream respiration. *Ecological Modelling* **117** (2–3), 333–342.
- Quan, D., Zhang, S., Shi, X. H., Sun, B., Song, S. & Guo, Z. Y. 2020 Impact of water environment factors on eutrophication status of Lake Ulansuhai based on monitoring data in 2013–2018. *Journal of Lake Sciences* **32** (06), 1610–1619.
- Sánchez, E., Colmenarejo, M. F., Vicente, J., Rubio, A., García, M. G., Travieso, L. & Borja, R. 2007 Use of the water quality index and dissolved oxygen deficit as simple indicators of watersheds pollution. *Ecological Indicators* **7** (2), 315–328.
- Schurr, J. M. & Ruchti, J. 1977 Dynamics of O₂ and CO₂ exchange, photosynthesis, and respiration in rivers from time-delayed correlations with ideal sunlight. *Limnology and Oceanography* **22** (2), 208–225.
- Song, S., Li, C., Shi, X., Zhao, S., Tian, W., Li, Z., Bai, Y., Cao, X., Wang, Q., Huotari, J., Tulonen, T., Uusheimo, S., Leppäranta, M., Loehr, J. & Arvola, L. 2019 Under-ice metabolism in a shallow lake in a cold and arid climate. *Freshwater Biology* **64** (10), 1710–1720.
- Steele, J. H. 1962 Environmental control of photosynthesis in the sea. *Limnology and Oceanography* **7** (2), 137–150.
- Stefan, H. G. & Fang, X. 1994 Dissolved oxygen model for regional lake analysis. *Ecological Modelling* **71** (1–3), 37–68.
- Sun, B., Li, C. Y., Zhang, S., Zhou, L. W. & Yang, Z. Y. 2009 Analysis of occurrence factors of supersaturated dissolved oxygen in Main Drainage Channel in the Hetao Irrigation District. *Environmental Chemistry* **28** (03), 449–450.
- Terry, J. A., Sadeghian, A. & Lindenschmidt, K. E. 2017 Modelling dissolved oxygen/sediment oxygen demand under ice in a shallow eutrophic prairie reservoir. *Water* **9** (2), 131.
- Thomann, R. V. & Mueller, J. A. 1987 *Principles of Surface Water Quality Modeling and Control*. Harper & Row Publishers, United States.
- Woszczyk, M., Bechtel, A. & Cieśliński, R. 2011 Interactions between microbial degradation of sedimentary organic matter and lake hydrodynamics in shallow water bodies: insights from Lake Sarbsko (northern Poland). *Journal of Limnology* **70** (2), 293.
- Xu, Z. & Xu, Y. J. 2015 Determination of trophic state changes with diel dissolved oxygen: a case study in a shallow lake. *Water Environment Research* **87** (11), 1970–1979.
- Xu, Z. & Xu, Y. J. 2016 A deterministic model for predicting hourly dissolved oxygen change: development and application to a shallow eutrophic lake. *Water* **8** (2), 41.
- Xu, H., Xu, M., Li, Y., Liu, X., Guo, L. & Jiang, H. 2018 Characterization, origin and aggregation behavior of colloids in eutrophic shallow lake. *Water Research* **142**, 176–186.

- Yu, R. H., Liu, T. X., Xu, Y. P. & Li, C. Y. 2007 The impacts of human activities on the Ulansuhai wetland environment. *Journal of Lake Sciences* **19** (04), 465–472.
- Zhu, Y. H., Zhang, S., Zhao, S. N., Tian, Q. Q., Han, Z. M. & Hu, J. F. 2017 Analysis of shallow water lake bogginess and causes in Lake Ulansuhai. *Water Resources Protection* **33** (05), 69–74.
- Zhu, L., Li, X., Zhang, C. & Duan, Z. 2017 Pollutants' release, redistribution and remediation of black smelly river sediment based on re-suspension and deep aeration of sediment. *International Journal of Environmental Research and Public Health* **14** (4), 374.
- Zison, S. W. 1978 *Rates, Constants, and Kinetics Formulations in Surface Water Quality Modeling*. Environmental Protection Agency, Office of Research and Development, Environmental Research Laboratory, United States.

First received 8 December 2021; accepted in revised form 13 May 2022. Available online 27 May 2022